Damage detection and localization algorithm using a dense sensor network of thin film sensors.

Austin Downey[a], Filippo Ubertini[b] and Simon Laflamme[a,c]

[a]Department of Civil, Construction, and Environmental Engineering, Iowa State University, Ames, IA, USA;
[b]Department of Civil and Environmental Engineering, University of Perugia, Perugia, Italy;
[c]Department of Electrical and Computer Engineering, Iowa State University, Ames, IA, USA;

ABSTRACT

Full Abstract

The authors have recently proposed a hybrid dense sensor network consisting of a novel, capacitive-based thin-film electronic sensor for monitoring strain on mesosurfaces and fiber Bragg grating sensors for enforcing boundary conditions on the perimeter of the monitored area. The thin-film sensor monitors local strain over a global area through transducing a change in strain into a change in capacitance. In the case of bidirectional in-plane strain, the sensor output contains the additive measurement of both principal strain components. When combined with the mature technology of fiber Bragg grating sensors, the hybrid dense sensor network shows potential for the monitoring of mesoscale systems. In this paper, we present an algorithm for the detection, quantification, and localization of strain within a hybrid dense sensor network. The algorithm leverages the advantages of a hybrid dense sensor network for the monitoring of large scale systems. The thin film sensor is used to monitor strain over a large area while the fiber Bragg grating sensors are used to enforce the uni-directional strain along the perimeter of the hybrid dense sensor network. Orthogonal strain maps are reconstructed by assuming different bidirectional shape functions and are solved using the least squares estimator to reconstruct the planar strain maps within the hybrid dense sensor network. Error between the estimated strain maps and measured strains is extracted to derive damage detecting features, dependent on the selected shape functions. Results from numerical simulations show good performance of the proposed algorithm.

Keywords: structural health monitoring, capacitive-based sensor, soft elastomeric capacitor, flexible membrane sensor, sensor network, signal decomposition, damage detection, damage localization, data fusion.

1. INTRODUCTION

Localization of damage on mesostructures including civil, aerospace and wind turbine blades, offer a substantial challenge to the advancement of structural health monitoring (SHM) due to their complex geometry and large size. Effective monitoring solutions for mesoscale structures need to be capable of monitoring the structures global (e.g. changing load paths, loss in global stiffness) and local (e.g. crack propagation, composite delamination) conditions. However, current sensing technologies and practices limit the distinction between localized and global faults on a mesoscale system.[1,2] Of particular interest to the authors is SHM and prognostics and health management (PHM) of wind turbine blades, where condition based maintenance (CBM) has demonstrated cost savings.[3–5] Additionally, the use of PHM can enable smart loads management for damaged wind turbine blades, resulting in increased blade life and a higher rate of return for wind turbine operators.[6]

Traditional approaches for SHM of wind turbine blades have focused on the global monitoring of structures using a limited number of sensors and applying a variety of post-processing techniques.[7–9] These techniques often lack the ability to localize damage and distinguish local failures from global events. Additionally, the large amounts of data collected and retained for many post-processing techniques can add unacceptable data

Further author information: (Send correspondence to Austin Downey)
Austin Downey: E-mail: adowney2@iastate.edu

Sensors and Smart Structures Technologies for Civil, Mechanical, and Aerospace Systems 2017,
edited by Jerome P. Lynch, Proc. of SPIE Vol. 10168, 1016813 · © 2017 SPIE
CCC code: 0277-786X/17/$18 · doi: 10.1117/12.2261408

storage costs.[10] The authors have recently proposed a solution to local/global detection problems with the concept of a hybrid dense sensor network of thin-film strain sensors combined with state-of-the-art strain gauges, where the thin-film sensors are used to cover the large area of the blade and state-of-the-art strain gauges (e.g., resistive strain gauges or fiber Bragg grating) for the purpose of updating boundary conditions.[11] The problem of optimized sensor placement within the HDSN has also been addressed.[12] This work purposes a data fusion technique that integrates data from the HDSN into a damage detection feature that is specially formulated for use in the SHM of mesoscale systems.

The goal of data fusion is to integrate sensor data from a multitude of sources in order to make a useful representation of the monitored systems that is capable for use in forming a damage detection decision. The resulting damage detection decision should be precise and less affected by outliers than what is possible through the monitoring of a single sensor. Additionally, data fusion can greatly reduce the magnitude of data that is retained for use in PHM. Data fusion may be performed to obtain an engineering parameter such as when relative information between various sensors is used to obtain mode shapes.[13] Additionally, as the main focus of this paper, data fusion can be used to obtain a feature from multiple sensors. Feature extraction is the process of building derived values (features) intended to be informative and non-redundant. In the case of SHM, these features should allow one to distinguish between a damaged and an undamaged state in a structure. Examples found in the literature are most commonly based on measured dynamic signals such as resonant frequencies, mode shapes, or properties derived from mode shapes.[1,14] The implementation of an SHM system typically produces a large amount of data; while almost all feature extraction methods compress data through the building of derived features, the use of features that provide a high level of data compression is important in the monitoring of wind turbine blades with HDSN due to the high channel count.[11,15]

This work introduces a computationally efficient, data-driven damage detection, quantification, and localization technique that is capable of monitoring mesostructures without associated models or historical datasets. More specifically, the proposed algorithm, termed NeRF (Network Reconstruction Feature), is capable of classifying HDSN sections into healthy or potentially damaged elements. This work uses HDSNs consisting of SECs for covering a large areas, and Fiber Bragg grating (FBG) sensors for the enforcement of boundary conditions and the separation of the area into sections. The SEC is used throughout this work as a large area electronic (LAE) strain transducer. Nevertheless, similarly developed LAEs optimized for strain measurements could also be used.[16–18]

The NeRF algorithm works through comparing an individual sensor state to an estimated response that is constructed through the fusion of multiple sensors arranged in an HDSN configuration. The estimated strain response is built by first assuming a shape function and using a least squares estimator (LSE) to approximate uni-directional strain maps within the HDSN. Thereafter, an error function is defined as the mean square error (MSE) with units of ϵ^2 between the measured and estimated strains at sensor locations. Features are defined as the change in error associated with a given increase in the shape function's complexity. This technique works to fuse the SEC and FBG strain data into a single damage detection feature, providing a simple and robust method for inspecting large numbers of sensors without the need for a complex model-driven approaches.

The contributions of this work are threefold: 1) a damage detection feature that integrates data from an HDSN into a single detection value; 2) a demonstration of the damage detection feature's ability to detect, quantify and localize damage; and 3) the evaluation of the damage detection feature's capabilities without relying on models or historical datasets. This paper is organized as follows. Section 2 introduces the SEC along with relevant background including the strain decomposition algorithm previously developed. Section 3 introduces simulations of the NeRF algorithm used for validation. Section 4 discusses simulation results. Section 5 concludes the paper.

2. BACKGROUND

This section provides the background on the SEC sensor, including its electro-mechanical model, along with the enhanced LSE-based algorithm for strain map decomposition.

2.1 Soft Elastomeric Capacitor

The SEC is a highly elastic thin-film sensor that transduces a change in its geometry (i.e., the monitored substrate's strain) into a measurable change in capacitance. It is fabricated from an SEBS block co-polymer matrix where the dielectric is filled with titania to increase both its durability and permittivity, while the conductive plates are fabricated from an SEBS filled with carbon black particles. The fabrication process of the SEC is documented in.[19] The SEC utilizes commercially available and inexpensive materials and is based on simple fabrication processes in its manufacturing, making the technology highly scalable.

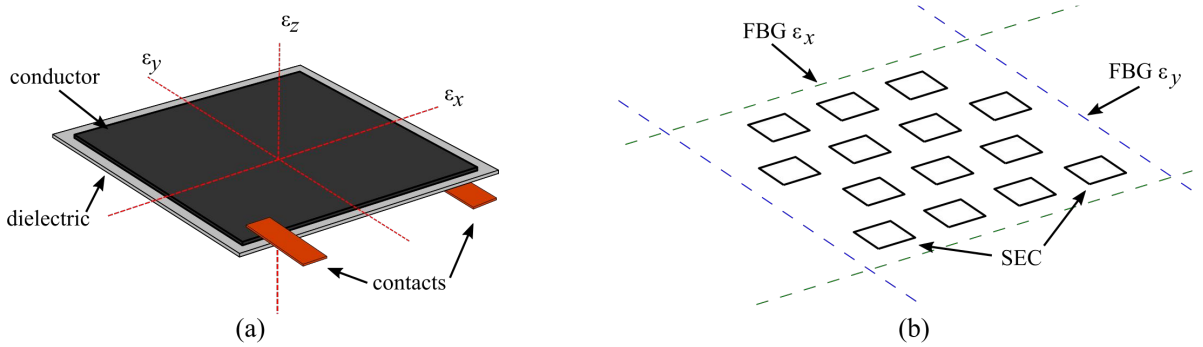

Figure 1: HDSN technology: (a) annotated SEC sensor with reference axes; and (b) HDSN section consisting of FBG sensors enforcing strain boundary conditions and SECs providing large area sensing coverage.

An SEC is adhered to the monitored substrate using a commercial two-part epoxy and is applied under tension to improve performance under compression. The SEC measures in-plane strain ($x-y$ plane in Fig. 1(a)). Assuming a low sampling rate (< 1 kHz), the SEC can be modeled as a non-lossy capacitor with capacitance C, given by the parallel plate capacitor equation,

$$C = e_0 e_r \frac{A}{h} \tag{1}$$

where $e_0 = 8.854$ pF/m is the vacuum permittivity, e_r is the polymer relative permittivity, A is the overlapping area of the conductive electrodes and h is the thickness of the dielectric.

Assuming small, in-plane strain, an expression relating the sensor's change in capacitance ΔC to the substrate's surface strain can be expressed

$$\frac{\Delta C}{C} = \lambda(\varepsilon_x + \varepsilon_y) \tag{2}$$

where $\lambda = 1/(1-\nu)$ represents the gauge factor of the sensor. For SEBS, $\nu \approx 0.49$, yielding a gauge factor $\lambda \approx 2$. The electro-mechanical model is derived in reference.[20] Eq. (2) shows that the signal of the SEC varies as a function of the orthogonal strain components $\varepsilon_x + \varepsilon_y$. The linearity of the electro-mechanical model has been validated for mechanical responses under 15 Hz.[20] For mechanical responses up to 40 Hz, an altered electro-mechanical model is presented in[21] but is not shown here for brevity. The SEC's electro-mechanical model has been validated for both static and dynamic strain and is presented in references.[19–21]

2.2 Strain Decomposition Algorithm

Orthogonal strain maps can be obtained from the additive strain measured by the SEC, as expressed in Eq. (2), using a network of sensors in combination with enforceable boundary conditions. Leveraging an HDSN configuration, the enforcement of boundary conditions relies on linear strain measurement techniques. In particular, FBG sensors are used in this work for updating the HDSN at key locations. The algorithm, termed the enhanced LSE algorithm, is presented in reference[11] and summarized in what follows.

The enhanced LSE algorithm starts by assuming a parametric displacement shape function. A p^{th} order polynomial is selected as the displacement shape function due to its mathematical simplicity and its ability to map a wide range of displacement topographies. The shape function is developed for the x-y plane with a constant plate thickness c, such that the deflection shape w is expressed as

$$w\left(x,y\right)=\sum_{i=1,j=1}^{p}b_{ij}x^{i}y^{j} \tag{3}$$

where $b_{i,j}$ are regression coefficients. Considering an HDSN with m sensors, which includes both SEC and FBG sensor nodes, displacements at sensor locations can be collected in a vector $\mathbf{W}=\left[\begin{array}{cccccc} w_1 & \cdots & w_k & \cdots & w_m \end{array}\right]^T=\mathbf{HB}$. Matrix $\mathbf{H}$ encodes information on sensor locations and vector $\mathbf{B}$ contains the regression coefficients such that $\mathbf{B}=\left[\begin{array}{ccc} b_1 & \cdots & b_f \end{array}\right]^T$ where b_f represents the last regression coefficient.

Appropriately defined diagonal weight matrices $\mathbf{\Gamma}$ are introduced into the $\mathbf{H}$ matrix such that $\mathbf{H}$ is defined as $\mathbf{H}=[\mathbf{\Gamma}_{\text{x}}\mathbf{H}_{\text{x}}|\mathbf{\Gamma}_{\text{y}}\mathbf{H}_{\text{y}}]$. $\mathbf{\Gamma}_x$ and $\mathbf{\Gamma}_y$ hold sensor weight values, and are formed with scalars $\gamma_{x,k}$ and $\gamma_{y,k}$ associated with the k-th sensor. For instance, an FBG node k orientated to make strain measurements in the x direction will take weight values $\gamma_{x,k}=1$ and $\gamma_{y,k}=0$. The following matrices are developed from quantities contained in (3):

$$\mathbf{H}_{\text{x}}=\mathbf{H}_{\text{y}}=\left[\begin{array}{cccc} y_1^n & x_1y_1^{n-1} & \cdots & x_1^{n-1}y_1 & x_1^n \\ y_m^n & x_my_m^{n-1} & \cdots & x_m^{n-1}y_m & x_m^n \end{array}\right] \tag{4}$$

Linear strain functions ε_x and ε_y along the x and y directions, respectively, can be obtained from Eq. (3) through the enforcement of Kirchhoff's plate theory as

$$\varepsilon_x(x,y)=-\frac{c}{2}\frac{\partial^2 w(x,y)}{\partial x^2}=\mathbf{\Gamma}_{\text{x}}\mathbf{H}_{\text{x}}\mathbf{B}_{\text{x}} \tag{5}$$

$$\varepsilon_y(x,y)=-\frac{c}{2}\frac{\partial^2 w(x,y)}{\partial y^2}=\mathbf{\Gamma}_{\text{y}}\mathbf{H}_{\text{y}}\mathbf{B}_{\text{y}} \tag{6}$$

with $\mathbf{B}=[\mathbf{B}_{\text{x}}|\mathbf{B}_{\text{y}}]^T$.

Thereafter, a signal vector $\mathbf{S}$ is constructed in terms of the sensors strain signal $\mathbf{S}=\left[\begin{array}{ccccc} s_1 & \cdots & s_k & \cdots & s_m \end{array}\right]^T$ where $\mathbf{S}$ contains the additive SECs and unidirectional FBGs strain measurements. The regression coefficient matrix $\mathbf{B}$ can now be estimated using an LSE:

$$\hat{\mathbf{B}}=(\mathbf{H}^T\mathbf{H})^{-1}\mathbf{H}^T\mathbf{S} \tag{7}$$

where the hat denotes an estimation. The estimated strain maps are reconstructed using

$$\hat{\mathbf{E}}_{\text{x}}=\mathbf{\Gamma}_{\text{x}}\mathbf{H}_{\text{x}}\hat{\mathbf{B}}_{\text{x}}\qquad\hat{\mathbf{E}}_{\text{y}}=\mathbf{\Gamma}_{\text{y}}\mathbf{H}_{\text{y}}\hat{\mathbf{B}}_{\text{y}} \tag{8}$$

where $\hat{\mathbf{E}}_{\text{x}}$ and $\hat{\mathbf{E}}_{\text{y}}$ are vectors containing the estimated strain in the x and y directions, respectively.

An HDSN without a sufficient number of uniaxial inputs will result in $\mathbf{H}$ being multi-collinear because $\mathbf{H}_{\text{x}}$ and $\mathbf{H}_{\text{y}}$ share multiple rows, resulting in $\mathbf{H}^T\mathbf{H}$ being non-invertible. Additionally, $\mathbf{H}^T\mathbf{H}$ may lack sufficient information to be invertible for a given shape function complexity. Therefore, ensuring a sufficient level of input information in the form of sensor signals or providing a shape function of limited complexity result in $\mathbf{H}^T\mathbf{H}$ being invertible.

3. METHODOLOGY

This section presents the proposed NeRF algorithm, along with the simulation parameters used for the validation of the algorithm performance.

3.1 Network Reconstruction Feature (NeRF)

Consider a section of an HDSN, similar to that shown in Fig. 1(b) consisting of FBG sensors along the perimeter and SECs placed within. To establish the NeRF's theoretical foundation, consider first the ideal situation where strain maps are easily approximated through the use of lower order shape functions. The error in the approximation, calculated at the sensor locations can be determined as:

$$\mathbf{V} = \frac{1}{n}\sum_{k=1}^{n}(\mathbf{S}_k - \mathbf{S}'_k)^2 \tag{9}$$

where $\mathbf{V}$ is a matrix of MSE values, $\mathbf{S}_k$ is the sensor signal, and $\mathbf{S}'_k$ is the LSE-estimated sensor signal using the reconstructed strain maps. The estimated sensor signals for FBG sensors measuring ε_x and ε_y are taken from $\hat{\mathbf{E}}_{\mathrm{x}}$ and $\hat{\mathbf{E}}_{\mathrm{y}}$, respectively, whereas estimated sensor signals for SECs are taken as the summation of $\hat{\mathbf{E}}_{\mathrm{x}}$ and $\hat{\mathbf{E}}_{\mathrm{y}}$ at the sensor locations, as shown in Eq. 2. This process is schematized in Fig. 3 where the orthogonal strain maps are created using the enhanced LSE algorithm outlined in red. The development of features is discussed in the upcoming subsection.

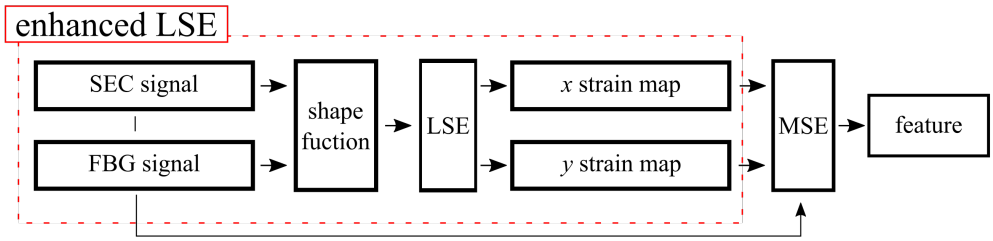

Figure 2: Network reconstruction feature (NeRF) algorithm.

From the approach presented above, it follows that strain fields with relatively simple strain topology will result in estimated strain maps that are capable of reconstructing the strain field with low levels of error. However, the introduction of a damage into the monitored substrate will result in locally more complex strain topologies resulting in higher levels of error at the measured sensors. The proposed algorithm is capable of detecting changes in the monitored substrate that are not directly monitored (i.e., covered by an SEC sensor) through monitoring the structural response around a localized damage case. This technique adds versatility to the proposed HDSN for monitoring mesoscale structures, such as wind turbine blades, by reducing the number and density of required sensors.

3.2 Feature extraction

Using the shape function shown in Eq. (3), the damage features for NeRF are taken as the change in sensor error ($\mathbf{V}$ that result from adding to the complexity of the shape function. Starting with $w(x,y) = \sum_{i=1,j=1}^{2} b_{ij}x^i y^j$, binomial shape function components are added in symmetric pairs from the outside of Pascal's triangle and progressing inwards for a given row. Therefore, feature No. 1 becomes the difference in reconstruction error, $\mathbf{V}$, between the polynomial shape functions $w(x,y) = \sum_{i=1,j=1}^{2} b_{ij}x^i y^j$ and $w(x,y) = \sum_{i=1,j=1}^{2} b_{ij}x^i y^j + x^3 + y^3$; feature No. 2 is the difference between $w(x,y) = \sum_{i=1,j=1}^{2} b_{ij}x^i y^j + x^3 + y^3$ and $w(x,y) = \sum_{i=1,j=1}^{2} b_{ij}x^i y^j + x^3 + y^3 + x^2 y + xy^2$, and so forth. The features used in this study and their nomenclature are listed in table 1. Note that no deflection displacement boundary conditions are enforced into the shape function. Instead, all boundary conditions are enforced into strain topography through the use of the uni-directional FBG sensors. The development of features from each HDSN section provides a high level of data compression from the fusion of all sensor signals $\mathbf{S}$ into a single feature-based scalar.

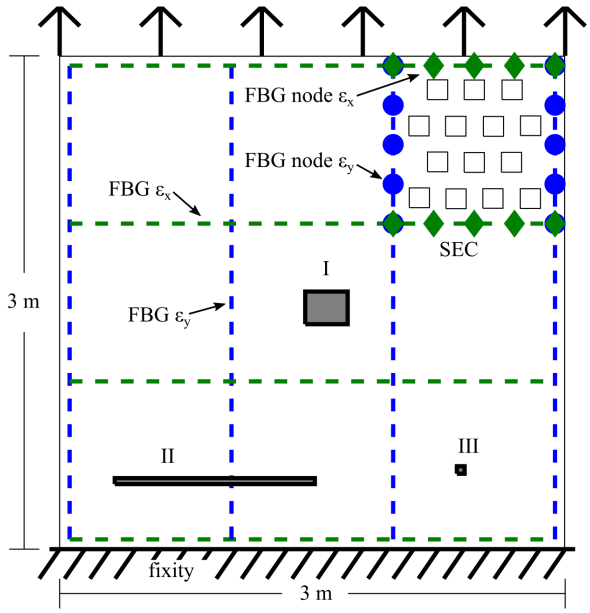

Figure 3: Rectangular cantilever plate under tensile loading with an HDSN split into nine sections used for algorithm validation.

Table 1: Polynominal complexities used for condition assessment features.

No.	term added	No.	term added
1	$x^3,\ y^3$	8	$x^3y^2,\ x^2y^3$
2	$x^2y,\ xy^2$	9	$x^6,\ y^6$
3	$x^4,\ y^4$	10	$x^5y,\ xy^5$
4	$x^3y,\ xy^3$	11	$x^7,\ y^7$
5	$x^2\ y^2$	12	$x^6y,\ xy^6$
6	$x^5,\ y^5$	13	$x^5y^2,\ x^2y^5$
7	$x^4y,\ xy^4$	14	$x^4y^3,\ x^3y^4$

3.3 Simulations

The NeRF algorithm is validated through simulations of a large cantilever plate under a uniform tensile loading of 45 kN/m, illustrated in Fig. 3. Nine HDSN sections are used to assess the effectiveness of the proposed NeRF system at damage detection and localization. The HDSN sections are constructed with networks of 14 SECs divided by unbroken strands of continuous FBG sensors measuring either ε_x or ε_y as denoted in Fig. 3. SECs are placed on an offset grid to introduce a level of complexity into $\mathbf{H}^T\mathbf{H}$ following preliminary results suggesting that this configuration may increase the HDSNs ability to detect damage that is not directly monitored by an SEC. Sensors are positioned with a slight randomness of ± 2 cm to account for simulated error in placement and to add a small amount of non-uniformity to the HDSN to better approximate an in-situ installation. For the same purpose, FBGs are placed along the x and y axes with a small gap around the edge. Noise is introduced into the sensors assuming a Gaussian normal distribution with noise levels of $25 \pm \mu\varepsilon$ for the SECs (based on previous study[22]) and $\pm 5\ \mu\varepsilon$ for the FBG nodes, representing a typical low resolution for FBG systems.[23]

The performance of the algorithm is investigated under three damage cases, illustrated in Fig. 3: I) large damage in an of area of relativity simple strain topography; II) large damage spanning two HDSN sections; and III) small damage in an area of relatively complex strain maps that is located between SEC sensors. Damage

Table 2: HDSN and FEA configurations.

HDSN sections	9	FEA elements	shell
SECs	126	integration points	9
SEC size	120 cm^2	elements	25372
FBG points	104	density	2 kg/mL
FBG points (ε_x)	52	Youngs modulus	20 GPA
FBG points (ε_y)	52	thickness	7 cm

case III was selected to demonstrate the limitations of the NeRFs algorithm. Each damage case consists of a delamination introduced as a 50% reduction in stiffness for the affected area. A stiffness reduction of 25% was also introduced for damage case I to determine the ability of the NeRF algorithm to quantify the extent of damage. Table 2 lists model-specific data relating to the finite element model and the simulated HDSN.

4. RESULTS

This section presents and discusses the simulation results for the validation of the NeRF algorithm. First, an HDSN section is inspected to develop features from the reconstructed strain maps. Thereafter, damage quantification results are presented for damage case I, followed by damage location results for cases I-III.

4.1 NeRF features

Consider the HDSN section that contains damage case I for both the healthy and damaged state. Figure 4(a) denotes the level of error (obtained through Eq. 9) as a function of the features listed in Table 1. The healthy state (solid black line in conjunction with the left axis) converges after a few added features, demonstrating that the strain topography can be easily reproduced with a relatively simple shape function. In comparison, damage case I (dashed red line in conjunction with the right axis) starts with a considerably higher level of strain and continuously benefits from adding more complexity to the shape functions. In both cases, the shape function beyond that produced by feature No. 14 became overly complex, whereas $\mathbf{H}^T\mathbf{H}$ becomes non-invertible. Therefore, solving for higher shape function with greater complexity would require additional sensors be added into the HDSN section.

The MSE on $\mathbf{V}$ and condition assessment feature corresponding to the change in $\mathbf{V}$ as a function of polynomial complexities (table 1) are presented in Fig. 4(a) for the healthy and damage cases. The damaged system results in higher condition assessment features at higher polynomial complexities. This is to be expected, as the mapping of strain around damage would typically require a more complex strain shape function. In comparison, mapping strain for the healthy state can be conducted using lower order polynomials as seen from the higher condition assessment features.

4.2 Quantification

Condition assessment features can be used to quantify different levels of damage as presented in Fig. 4(b). Here, features from polynomial complexities No. 3 and 13 are used to distinguish varying levels of stiffness damage present in damage case I. Feature scatters increase as the damage level increases, as expected given that the LSE encounters more variation with increase in topology complexity. Feature distance can be any n-dimensional combination of NeRF. However, a two-dimensional feature distance is shown here for simplicity. A two-dimensional Gaussian distribution for 2σ, σ being the standard deviation, is plotted over the scatter plot to provide a level of confidence for the feature extraction.

4.3 Localization

Damage localization is conducted in terms of feature distances. Results shown in Fig. 5 are expressed in terms of such feature distances, taken as the Euclidean distance between the center of the Gaussian cluster, as illustrated in Fig. 4(b), derived from feature No. 6, 9 and 11 and the axes origin. Figure 5(a) presents the healthy state of the plate while Fig. 5(b-d) present damage cases I-III, respectively. Figure 5(a) demonstrates that a more complex strain topology is located at the fixity of the place. These results are to be expected as the fixity

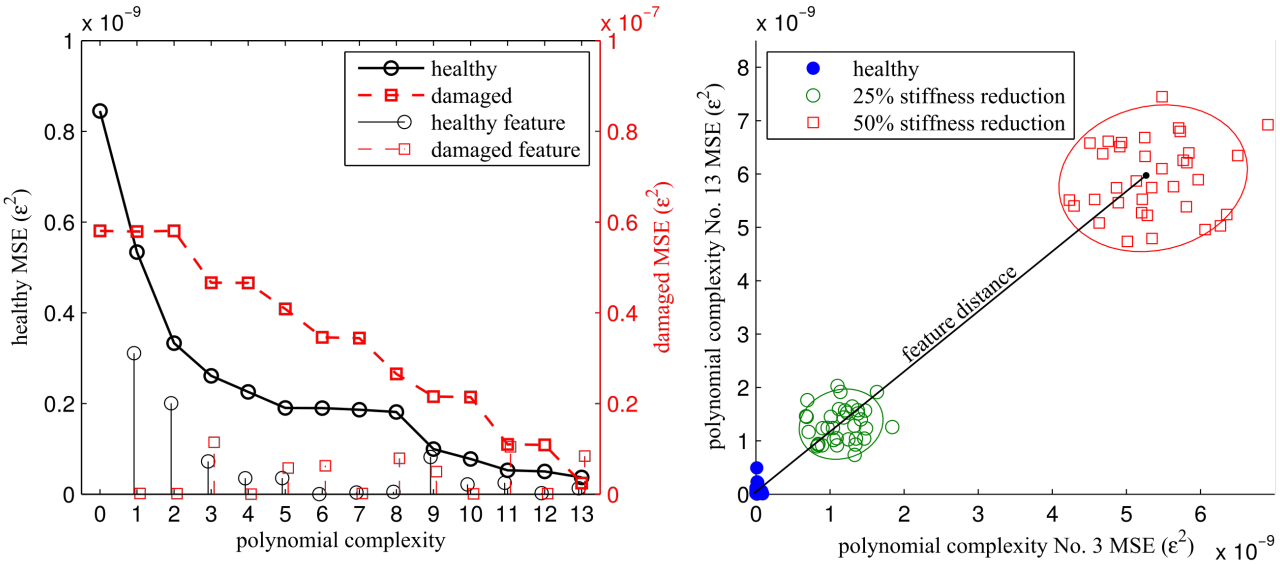

Figure 4: NeRF: (a) MSE of $\mathbf{V}$ as a function of polynomial complexity; and (b) clustering of features for damage quantification.

will result in highly curved local strain fields. The non-symmetric relationship is most likely a result of the slight randomness applied to individual SEC layouts, resulting in non-identical HDSN sections. Damage case I is presented in Fig. 5(b). Here, the location of a high strain map reconstruction error $\mathbf{V}$ is easily detectable as the error caused by the damage case is significantly higher than that present along the fixed edge. This sharp increase in error demonstrates the NeRF algorithm's ability to distinguish between HDSNs that may be damaged from those that are healthy. This damage case is detectable without the use of historical data or external models as under the current loading condition, the HDSN section in the middle of the plate should be in close agreement with its neighbors.

The algorithm's robustness to multiple damaged sections is presented in Fig. 5(c). Here, damage is introduced across two HDSN sections (illustrated in Fig. 3). The feature distance results demonstrate that the algorithm is capable of detecting damage in both HDSN sections. Lastly, a more difficult damage case is introduced. Damage case III consists of a 50% reduction in stiffness for a 0.2% area of the HDSN section, positioned between SEC sensors. Feature distances are presented in Fig. 5(d). While the magnitude of the feature distance increased by approximately 1/3, form 1.95×10^{-9} (ε^2) for the undamaged state to 2.97×10^{-9} (ε^2) for the damages state damage, the assessment of damage is difficult because a complex strain topology is already present in the HDSN section of interest. This demonstrates a limitation of the NeRF. A solution would be to leverage an external model or historical data to reference the error to damage case III.

NeRF is capable of providing a high level of data compression in the form of features fused from sections of an HDSN. In the cantilever plate example, each feature or feature distance is the result of data fusion of 34 individual data channels. When extended to the entire plate, and considering that some FBG nodes are shared between sections, the NeRF algorithm provides a data compression of 246 data points to 9, equivalent to a 96.4% data reduction. Compression of data allows for faster post-processing, retention of longer historical datasets, and a reduction in the cost associated with building prognostic datasets.

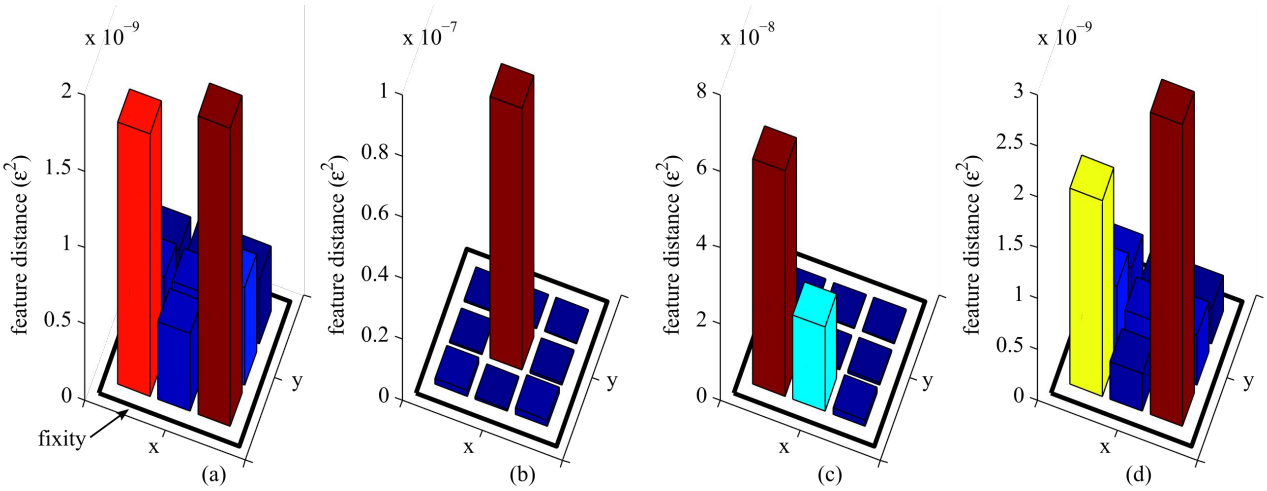

Figure 5: Damage localization for the square plate: (a) healthy case; (b) case I; (c) case II; (d) case III.

5. CONCLUSIONS

This work introduced a computationally efficient, data-driven damage detection, quantification and localization feature extraction technique that is capable of monitoring mesoscale structures such as wind turbine blades, without associated models or historical datasets. Termed the network reconstruction feature (NeRF), the algorithm allows for the separation of healthy and potentially damaged sections within a hybrid dense sensor network (HDSN). Specifically designed for use with high-count HDSN, NeRF provides data fusion for sensors within an HDSN section and outputs a single feature scalar providing a high level of data compression when implemented over a large structure. The NeRF algorithm works through assuming a shape function and using the LSE to approximate uni-directional strain maps within the HDSN. An error function, measured by the mean square error (MSE) between the sensors' measured and estimated strain is obtained. Features are defined as the change in error associated with a given increase in the shape function complexity. Data compression provided by the NeRF algorithm reduces the computational effort and storage space needed to develop and monitor prognostic datasets for large-scale structures.

Numerical investigations were conducted on a cantilever plate equipped with 126 SECs and 104 FBG nodes, sectioned into 9 discrete sections. The NeRF algorithm successfully distinguished between damaged and healthy HDSN sections for three different damage cases. In two damage cases, it was possible to distinguish between healthy and damaged conditions without the use of historical data. However, it was difficult to detect damage case III because it was highly localized within a region of high strain complexity. Its detection would likely require the comparison with the undamaged case (i.e., historical data set). Future investigations are needed to validate the algorithm for use with an extended library of loading and damage cases. Sensor network design and partitions, including the number and of SECs within HDSN sections, also needs exploration. This includes the use of asymmetric sensor networks and the inclusion of SECs of different geometries.

Results presented show the promise of the technology for monitoring large-scale surfaces, such as wind turbine blades and aircraft wings, by leveraging a hybrid sensor network configuration. For example, the HDSN data could be used to monitor wind turbine blades in both global and local conditions, whereas the NeRF algorithm could be used to formulate prognostic datasets to detect changes in structural health over time, reducing wind turbines operational cost through the use of damage mitigation technology and real-time structural health management.

Acknowledgements

This work is supported by the National Science Foundation Grant No. 1069283, which supports the activities of the Integrative Graduate Education and Research Traineeship (IGERT) in Wind Energy Science, Engineering and Policy (WESEP) at Iowa State University. Their support is gratefully acknowledged.

REFERENCES

1. Y Zou, LPSG Tong, and GP Steven. Vibration-based model-dependent damage (delamination) identification and health monitoring for composite structures-a review. *Journal of Sound and vibration*, 230(2):357–378, 2000.
2. Filippo Ubertini, Gabriele Comanducci, and Nicola Cavalagli. Vibration-based structural health monitoring of a historic bell-tower using output-only measurements and multivariate statistical analysis. *Structural Health Monitoring*, page 1475921716643948, 2016.
3. Chao Hu, Byeng D Youn, Pingfeng Wang, and Joung Taek Yoon. Ensemble of data-driven prognostic algorithms for robust prediction of remaining useful life. *Reliability Engineering & System Safety*, 103:120–135, 2012.
4. Douglas Adams, Jonathan White, Mark Rumsey, and Charles Farrar. Structural health monitoring of wind turbines: method and application to a hawt. *Wind Energy*, 14(4):603–623, 2011.
5. Peter C. Chang, Alison Flatau, and S. C. Liu. Review paper: Health monitoring of civil infrastructure. *Structural Health Monitoring*, 2(3):257–267, 2003.
6. Phillip W Richards, D Todd Griffth, and Dewey H Hodges. Smart loads management for damaged offshore wind turbine blades. *Wind Engineering*, 39(4):419–436, 2015.
7. Erik Gross, Todd Simmermacher, Mark Rumsey, and Rick I Zadoks. Application of damage detection techniques using wind turbine modal data. In *American Society of Mechanical Engineers Wind Energy Symp.(Reno, NV, USA)*, pages 99–0047, 1999.
8. Chia Chen Ciang, Jung-Ryul Lee, and Hyung-Joon Bang. Structural health monitoring for a wind turbine system: a review of damage detection methods. *Measurement Science and Technology*, 19(12):122001, 2008.
9. Mark A Rumsey and Joshua A Paquette. Structural health monitoring of wind turbine blades. In *The 15th International Symposium on: Smart Structures and Materials & Nondestructive Evaluation and Health Monitoring*, pages 69330E–69330E. International Society for Optics and Photonics, 2008.
10. Shinae Jang, Hongki Jo, Soojin Cho, Kirill Mechitov, Jennifer A Rice, Sung-Han Sim, Hyung-Jo Jung, Chung-Bang Yun, Billie F Spencer Jr, and Gul Agha. Structural health monitoring of a cable-stayed bridge using smart sensor technology: deployment and evaluation. *Smart Structures and Systems*, 6(5-6):439–459, 2010.
11. Austin Downey, Simon Laflamme, and Filippo Ubertini. Reconstruction of in-plane strain maps using hybrid dense sensor network composed of sensing skin. *Measurement Science and Technology*, 27(12):124016, nov 2016.
12. Austin Downey, Chao Hu, and LaFlamme Simon. Optimal sensor placement within a hybrid dense sensor network using an adaptive genetic algorithm with learning gene pool. *Structural Health Monitoring*, In press (2017).
13. Hoon Sohn, Charles R Farrar, Francois M Hemez, Devin D Shunk, Daniel W Stinemates, Brett R Nadler, and Jerry J Czarnecki. A review of structural health monitoring literature: 1996–2001. *Los Alamos National Laboratory, USA*, 2003.
14. Tian Han, Bo-Suk Yang, Won-Ho Choi, and Jae-Sik Kim. Fault diagnosis system of induction motors based on neural network and genetic algorithm using stator current signals. *International Journal of Rotating Machinery*, 2006, 2006.
15. Jingzhe Wu, Chunhui Song, Hussam S Saleem, Austin Downey, and Simon Laflamme. Network of flexible capacitive strain gauges for the reconstruction of surface strain. *Measurement Science and Technology*, 26(5):055103, apr 2015.
16. Andrew R Burton, Masahiro Kurata, Hiromichi Nishino, and Jerome P Lynch. Fully integrated patterned carbon nanotube strain sensors on flexible sensing skin substrates for structural health monitoring. In *SPIE Smart Structures and Materials+ Nondestructive Evaluation and Health Monitoring*, pages 98030S–98030S. International Society for Optics and Photonics, 2016.

17. Annibale Luigi Materazzi, Filippo Ubertini, and Antonella D'Alessandro. Carbon nanotube cement-based transducers for dynamic sensing of strain. *Cement and Concrete Composites*, 37:2–11, 2013.
18. Yao Yao and Branko Glisic. Detection of steel fatigue cracks with strain sensing sheets based on large area electronics. *Sensors*, 15(4):8088–8108, 2015.
19. Simon Laflamme, Matthias Kollosche, Jerome J. Connor, and Guggi Kofod. Robust flexible capacitive surface sensor for structural health monitoring applications. *Journal of Engineering Mechanics*, 139(7):879–885, jul 2013.
20. Simon Laflamme, Filippo Ubertini, Hussam Saleem, Antonella D'Alessandro, Austin Downey, Halil Ceylan, and Annibale Luigi Materazzi. Dynamic characterization of a soft elastomeric capacitor for structural health monitoring. *Journal of Structural Engineering*, 141(8):04014186, aug 2015.
21. Hussam Saleem, Austin Downey, Simon Laflamme, Matthias Kollosche, and Filippo Ubertini. Investigation of dynamic properties of a novel capacitive-based sensing skin for nondestructive testing. *Materials Evaluation*, 73(10):1384–1391, oct 2015.
22. Simon Laflamme, Hussam S. Saleem, Bharath K. Vasan, Randall L. Geiger, Degang Chen, Michael R. Kessler, and Krishna Rajan. Soft elastomeric capacitor network for strain sensing over large surfaces. *IEEE/ASME Transactions on Mechatronics*, 18(6):1647–1654, dec 2013.
23. Mousumi Majumder, Tarun Kumar Gangopadhyay, Ashim Kumar Chakraborty, Kamal Dasgupta, and Dipak Kumar Bhattacharya. Fibre bragg gratings in structural health monitoring-present status and applications. *Sensors and Actuators A: Physical*, 147(1):150–164, 2008.